Lecture Notes in Electrical Engineering 541

Yidong Gu
Ming Gao
Guangheng Zhao *Editors*

Proceedings of the Tiangong-2 Remote Sensing Application Conference

Technology, Method and Application

Springer

Lecture Notes in Electrical Engineering

Volume 541

Lecture Notes in Electrical Engineering (LNEE) is a book series which reports the latest research and developments in Electrical Engineering, namely:

- Communication, Networks, and Information Theory
- Computer Engineering
- Signal, Image, Speech and Information Processing
- Circuits and Systems
- Bioengineering
- Engineering

The audience for the books in LNEE consists of advanced level students, researchers, and industry professionals working at the forefront of their fields. Much like Springer's other Lecture Notes series, LNEE will be distributed through Springer's print and electronic publishing channels.

More information about this series at http://www.springer.com/series/7818

Yidong Gu · Ming Gao · Guangheng Zhao
Editors

Proceedings of the Tiangong-2 Remote Sensing Application Conference

Technology, Method and Application

Springer

Editors
Yidong Gu
Technology and Engineering Center
for Space Utilization, CAS
Beijing, China

Ming Gao
Technology and Engineering Center
for Space Utilization, CAS
Beijing, China

Guangheng Zhao
Technology and Engineering Center
for Space Utilization, CAS
Beijing, China

ISSN 1876-1100 ISSN 1876-1119 (electronic)
Lecture Notes in Electrical Engineering
ISBN 978-981-13-3500-6 ISBN 978-981-13-3501-3 (eBook)
https://doi.org/10.1007/978-981-13-3501-3

Library of Congress Control Number: 2018962984

This Springer imprint is published by the registered company Springer Nature Singapore Pte Ltd.
The registered company address is: 152 Beach Road, #21-01/04 Gateway East, Singapore 189721, Singapore

Organization

Expert Committee

Shancong Zhang	Technology and Engineering Center for Space Utilization (CSU), Chinese Academy of Sciences (CAS)
Congmin Lv	CSU, CAS
Xuzhi Li	CSU, CAS
Jun Wei	Shanghai Institute of Technical Physics, CAS
Yunhua Zhang	National Space Science Center, CAS
Shurong Wang	Changchun Institute of Optics, Fine Mechanics and Physics, CAS

Advisory Committee

Fang Shen	East China Normal University
Fuxiang Huang	National Satellite Meteorological Center
Guangjian Yan	Beijing Normal University
Ji Zhou	University of Electronic Science and Technology of China
Jihua Meng	Institute of Remote Sensing and Digital Earth, CAS
Jingjuan Liao	Institute of Remote Sensing and Digital Earth, CAS
Jinsong Chong	Institute of Electronics, CAS
Minzheng Duan	Institute of Atmospheric Physics, CAS
Pifu Cong	National Marine Environmental Monitoring Center
Qianguo Xing	Yantai Institute of Coastal Zone Research, CAS
Shudong Wang	Institute of Remote Sensing and Digital Earth, CAS
Wenquan Zhu	Beijing Normal University
Xiaofeng Yang	Institute of Remote Sensing and Digital Earth, CAS

Xiaoxian Huang	Shanghai Institute of Technical Physics, CAS
Xin Li	Anhui Institute of Optics and Fine Mechanics, CAS
Yong Zhang	National Satellite Meteorological Center
Yuchu Qin	Institute of Remote Sensing and Digital Earth, CAS
Yutian Fu	Shanghai Institute of Technical Physics, CAS
Zengxiang Zhang	Institute of Remote Sensing and Digital Earth, CAS
Zhengqiang Li	Institute of Remote Sensing and Digital Earth, CAS
Bo Zhong	Institute of Remote Sensing and Digital Earth, CAS
Dongdong Shao	Beijing Normal University
Hongyan Ren	Institute of Geographic Sciences and Natural Resources Research, CAS
Jian Chen	Nanjing University of Information Science and Technology
Jinyang Du	Institute of Remote Sensing and Digital Earth, CAS
Lingmei Jiang	Beijing Normal University
Liwei Li	Institute of Remote Sensing and Digital Earth, CAS
Lixin Dong	National Satellite Meteorological Center
Runhe Shi	East China Normal University
Shilin Tang	South China Sea Institute of Oceanology, CAS
Shuying Jin	Wuhan University
Xiaohuan Xi	Institute of Remote Sensing and Digital Earth, CAS
Yonghua Sun	Capital Normal University
Wei Chen	Institute of Remote Sensing and Digital Earth, CAS

Compiling Committee

Shengyang Li	CSU, CAS
Lingli Mu	CSU, CAS
Bangyong Qin	CSU, CAS
Kang Liu	CSU, CAS
Chunying Wu	CSU, CAS
Wanfeng Zhang	CSU, CAS
Zhiwen Liu	CSU, CAS
Hong Tan	CSU, CAS
Xue Wan	CSU, CAS

Contents

Earth Observation Payloads and Data Applications of Tiangong-2 Space Laboratory

Ming Gao(✉)

Key Laboratory of Space Utilization, Technology and Engineering Center for Space Utilization, Chinese Academy of Sciences, Beijing 100094, China
mgao@csu.ac.cn

Abstract. As China's first Space Laboratory, Tiangong-2 was designed to carry on a number of space scientific experiments and application tests. For the Earth observation, Tiangong-2 is equipped with Wide-band Imaging Spectrometer (WIS), Interferometric Imaging Radar Altimeter (InIRA) and Multi-band Ultraviolet Edge Imaging Spectrometer (MUEIS). Up to now, these earth observation payloads have acquired a large amount of data, which has been released and applied in many fields. In this paper, the working mechanism, technical characters and advantages of these payloads are introduced, and the data acquirement, processing and service are summarized. With the data accumulation and application promotion, a series of application results have emerged. Some typical application achievements are presented as well. In the future, the earth observation payloads will continue providing data, and more and more applications are prospected.

Keywords: Tiangong-2 · Earth observation payload
Wide-band Imaging Spectrometer · Interferometric Imaging Radar Altimeter
Multi-band Ultraviolet Edge Imaging Spectrometer · Data application

1 Introduction

Tiangong-2, successfully launched on September 15, 2016, is the first space laboratory in China [1]. It was designed to carry on a number of space scientific experiments and application tests, which represents the development direction of China's space science frontier and strategic high-technology [2]. The Schematic diagram of Tiangong-2 is shown as Fig. 1.

Tiangong-2 Space Laboratory carried on more tasks than those of Tiangong-1. Tiangong-2 boarded more than ten space scientific experiments and application tests, covering earth observation and space earth science, space astronomy, microgravity physics, microgravity fluid physics and space material science, space life science and space environment, etc. [4].

Y. Gu et al. (Eds.): *Proceedings of the Tiangong-2 Remote Sensing Application Conference,* LNEE 541, pp. 1–13, 2019.
https://doi.org/10.1007/978-981-13-3501-3_1

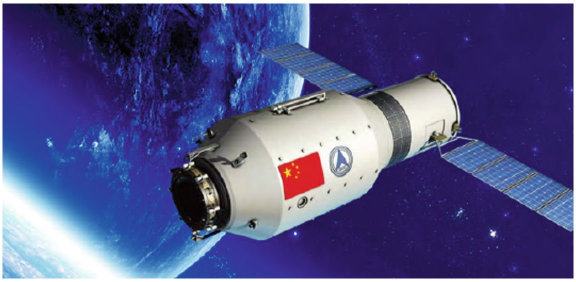

Fig. 1. Schematic diagram of Tiangong-2 Space Laboratory [3]

2 Earth Observation Payloads

The earth observation payloads on Tiangong-2 includes Wide-band Imaging Spectrometer (WIS), Interferometric Imaging Radar Altimeter (InIRA) and Multi-band Ultraviolet Edge Imaging Spectrometer (MUEIS) based on advanced technology [2]. These earth observation payloads have been playing an important role in such fields as land, ocean and atmosphere and so on [5].

2.1 Wide-Band Imaging Spectrometer

WIS is a new generation moderate resolution optical payload, with wide-band and wide field of view [4]. WIS contains 14 programmable visible and near-infrared spectral channels (0.40 μm ∼ 1.04 μm), 2 short wavelength infrared channels (1.232 μm ∼ 1.654 μm) and 2 thermal infrared channels (8.125 μm ∼ 9.275 μm). The ground resolution of each band in nadir point is 100 m, 200 m and 400 m respectively. WIS adopted push-broom and multi-module fields of view splicing imaging technology, with 300 km swath and 42° field of view [4]. WIS data are suitable for large-scale ground object detection, inland lake extraction, land and atmospheric monitoring, ocean and coastal water color monitoring, and water temperature observation, etc. [4]. The schematic diagram of WIS is shown as Fig. 2.

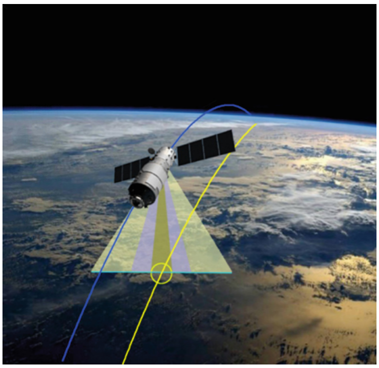

Fig. 2. Schematic diagram of on-orbit observation for WIS

2.2 Interferometric Imaging Radar Altimeter

InIRA uses small incidence angle to acquire high-precision ocean-land interference data, which can obtain echo signals of sea surface or terrestrial surface with high-coherence, based on receivers with dual-antenna and dual-channel [4]. It can extract the ocean interference phase map and three-dimensional ocean morphology. In the land applications, it also can obtain the three-dimensional topographic information. Figure 3 is the schematic diagram of on-orbit observation for InIRA Fig. 3. Schematic diagram of on-orbit observation for InIRA [1].

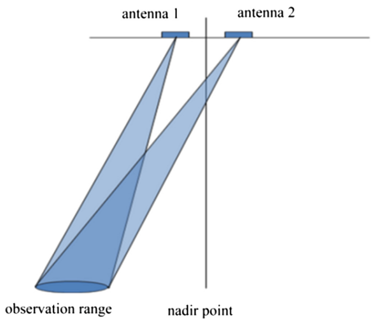

Fig. 3. Schematic diagram of on-orbit observation for InIRA [1]

The spatial resolution of InIRA in ocean interference model is 10 km × 10 km, with elevation precision is less than 8.2 cm (when orbital accuracy is less than 3 cm), and that in land model is 200 m × 200 m, with elevation precision is less than 10 m. The spatial resolution of the two-dimensional image is 100 m × 100 m.

InIRA data plays an important role in research of the global marine and land dynamic environment, including sea level altitude measurement, sea surface wind speed measurement, ocean currents monitoring, etc. [1].

2.3 Multi-band Ultraviolet Edge Imaging Spectrometer

MUEIS consists of Multi-Azimuth UV Imager (MAVI) and Front-azimuth Broadband Hyperspectrometer (FABH) [4].

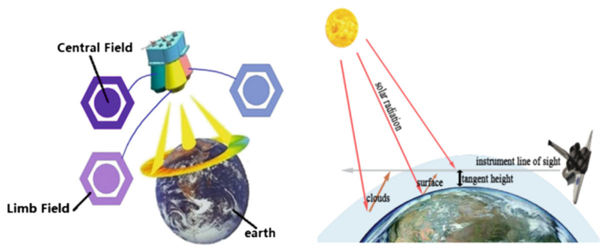

Fig. 4. Schematic diagram of on-orbit observation for MUEIS [6]

MAVI is used to detect radiation characteristics of the global mesosphere atmosphere with large field of view. FABH can provide precise spectral detection of atmosphere with over 120 channels. The schematic diagram is shown in Fig. 4.

MAVI has two fields of view with three channels (265 nm, 295 nm and 360 nm). One is central field used to detect the radiation brightness of whole atmosphere within 10 degrees of the nadir point, and the other one is limb field used to observe radiation brightness of the earth in six-azimuth with the field view about 140°. FABH with spectrum range of 290 nm ~ 1000 nm is used to detect the change of atmospheric precise spectrum change at different altitude from 10 km ~ 60 km [6].

MUEIS data is able to extract the vertical structure and three-dimensional dynamic distribution of atmospheric trace gases, atmospheric density, ozone distribution and aerosol, which can help human beings to understand the interaction between mesosphere and lower thermosphere, solar activity and space weather, as well as the relationship between earth weather and climate [4].

3 On-Orbit Operation

Since Tiangong-2 was successfully launched, it has been working for more than 2 years in a near-circular orbit with 340 km ~ 450 km height and 42° ~ 43° inclination [7]. The observation coverage range is between north 42° and south 42° latitude, shown in Fig. 5.

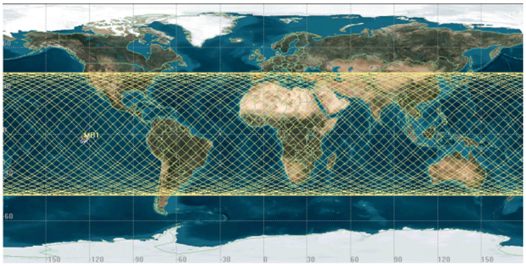

Fig. 5. The observation coverage range in Tiangong-2

At present, a large amount of high-quality image data have been obtained by Tiangong-2. Among them, the WIS standard data products are about 8.98 TB covering 119.1 million km^2. The InIRA data products are about 1.4 TB, with a global coverage of 33.97 million km^2. The standard data products of MUEIS are about 3.98 TB. Technology and Engineering Center for Space Utilization, Chinese Academy of Sciences (CSU) carries on data processing and generates amount of data products, shown in Table 1. All of data products are available on the website (http://www.msadc.cn/en).

Table 1. Standard data products of each earth observation payloads

Product Level	WIS	InIRA	MUEIS
Level 1	Radiometric correction products	Multiple-visual replica image products	Preprocessing products
Level 2	Geometric correction products	Geometric correction products	Primary atmospheric products
Level 3	Geometric correction products with high precision	Ortho-rectification products	None
Level 4	Ortho-rectification products	Three-dimensional elevation products	None
Level 5	General thematic products	None	None
Product format	Geo TIFF and XML	DAT/Geo TIFF and XML	HDF 5

4 Data Applications

With the data accumulation, plenty of data has been utilized in the fields of land and resource investigation, ocean and coastal zone monitoring, lake and farmland extraction, environment evaluation, etc. A series of application results have emerged, which showed great application potential.

4.1 The Applications of WIS

WIS data has been widely used in coastal zone change monitoring, lake extraction and change monitoring, land cover classification and change detection, environment monitoring and evaluation, crop identification, etc.

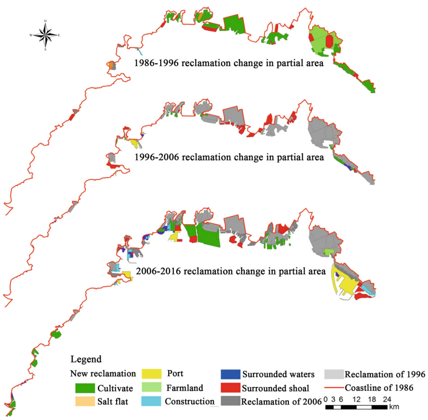

Fig. 6. Distribution of reclamation area in the Liaodong Bay

Coastal Zone Change Monitoring

Based on WIS data and other data, the researchers have carried out coastal zone change monitoring of Laizhou Bay, land change monitoring of Liaodong Bay (Fig. 6) [8], and Pearl River Estuary in the last 30 years.

The above applications reveal the spatial-temporal relationship between the coastal zone and the reclamation area in the Liaodong Bay. The result shows that it has the largest new reclamation area (266.55km2) in Linghai City of Liaoning Province in the past 30 years. The second largest one (226.13 km^2) is Dayi County of Liaoning Province [8].

Lake Extraction

The near-infrared data of WIS has also been used to extract water bodies and monitor change in Qinghai Lake, Poyang Lake, and Cuoqin County (Fig. 7).

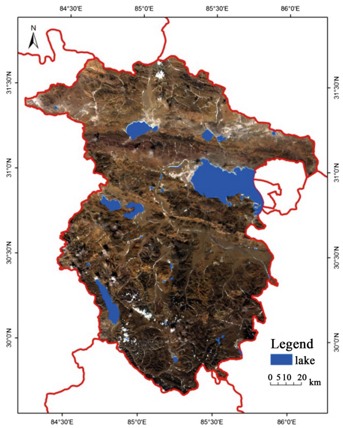

Fig. 7. Lake extraction in Cuoqin County, China

In Cuoqin, about 1254 km^2 of lake was extracted, and the identification accuracy was 93.74%. The near-infrared data of WIS shows the broad application prospects in water body extraction and change monitoring.

Land Cover Classification

In terms of land cover classification and change monitoring, the data of WIS was utilized in northwestern Mexico, Dongying City, Shandong Province (Fig. 8), and Nanjing City, Jiangsu Province, etc.

Using the data of WIS, the land cover classification of Dongying City has been carried out with accuracy of 84.5%. The spatial distribution of seven typical land cover in Dongying City was well extracted. Land cover classification results show that the near-infrared data of WIS contains a large amount of information suitable for high-precision land use classification.

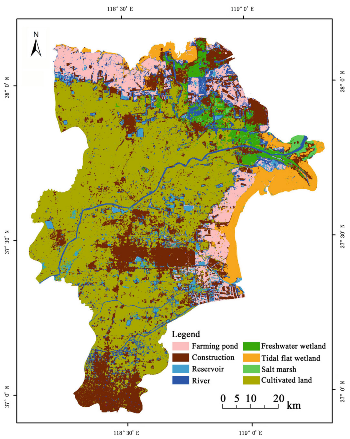

Fig. 8. Distribution of land cover types in Dongying, China

Ecological Environment Monitoring and Evaluation

At present, WIS data played an important role in wetland change monitoring in the Yellow River Delta and Panjin City, Liaoning Province [9]. Also the governments have used the data to identify algae in Taihu Lake and Chaohu Lake, and mangroves in the Beibu Gulf, Guangxi Province.

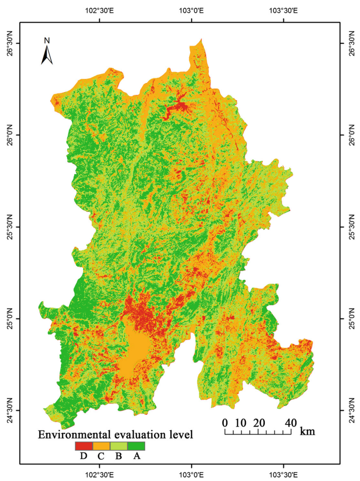

Fig. 9. Environment evaluation for Kunming City, China

As shown in Fig. 9, from A (green) to D (red), the environmental condition is reduced. In this application, area A is account for 62.75% of the total area of Kunming, which has a good ecological environment quality [10]. The monitoring and evaluation results reflect the ecological environment, which can provide decision support for the government to protect and restore ecological environment scientifically.

Crop Identification

In crop identification, the near-infrared data of WIS can reflect the planting structure and area, which provide support for yield evaluation. At present, the data had been used in cotton planting extraction in Hami, Xinjiang [11], winter wheat planting area extraction in Binzhou City and Dongying City, Shandong Province.

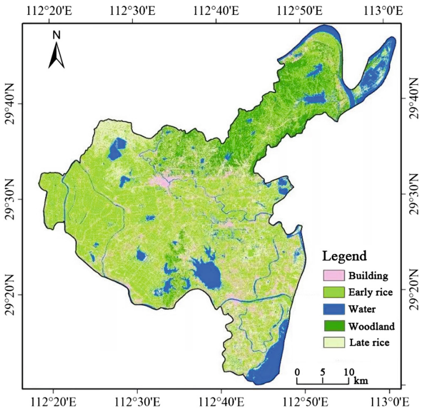

Fig. 10. Rice planting extraction of Huarong County, China

The spatial distribution of rice planting in Huarong, Hunan Province [12] is shown in Fig. 10. In this application, the planting area of early rice and later rice was extracted with high accuracy.

4.2 The Applications of InIRA

The data obtained by InIRA has been used in a large number of application researches on sea level altitude measurement, sea surface wind speed measurement, sea surface wavelength and wave inversion, ocean vortex detection, lake level inversion and so on. This paper takes the sea level altitude measurement and sea surface wind speed measurement as examples.

Sea level Altitude Measurement

Sea level altitude measurement result was obtained based on InIRA data. Figure 11 shows the InIRA elevation map of local sea level, the red line is shooting trajectory of 5° incident angle.

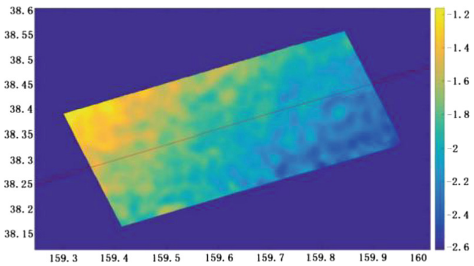

Fig. 11. InIRA elevation map of the local sea level in the Northwest Pacific

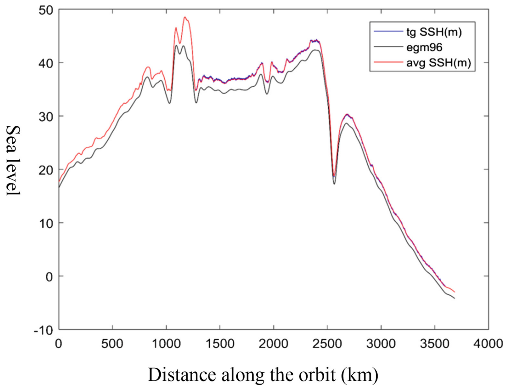

Fig. 12. Sea level altitude along the rail at 5° incident angle in the western Pacific

Figure 12 is the sea level altitude obtained by inversion of the position along the 5° incident angle. The blue line is the absolute elevation of the sea level derived from the InIRA data. The red line is the average of elevation in the corresponding area, and black line is the geoid. As shown in Fig. 12, the sea level altitude derived from InIRA data is consistent with the trend of the geoid.

Sea surface Wind Speed Measurement

Using the InIRA data obtained on September 22, 2016, the sea surface wind speed inversion in the North Atlantic Ocean is shown in Fig. 13.

Figure 14 showed the wind speed reanalysis result by US National Centers for Environmental Prediction. Comparing of Fig. 13 with Fig. 14, the measurement accuracy of InIRA is less than 2 m/s. In terms of sea surface wind speed measurement, InIRA data can provide effective support for ocean dynamics research.

4.3 The Applications of MUEIS

MUEIS data can be used to obtain radiation brightness image and atmospheric parameter information with high spatial, high time and high vertical resolution.

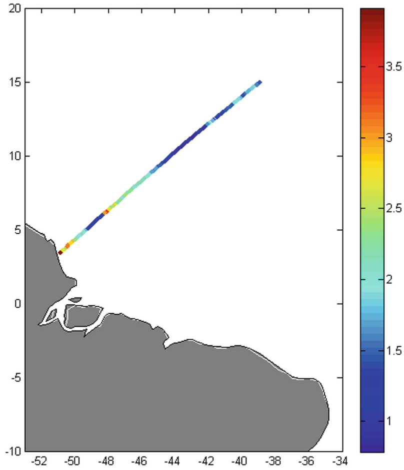

Fig. 13. Inversion of wind speed using InIRA data

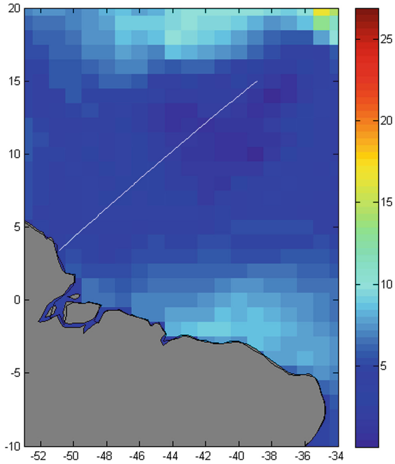

Fig. 14. Wind speed reanalysis result by NCEP (2016.09.22)

Furthermore, it can extract the vertical structure and three-dimensional dynamic distribution of atmospheric trace gases, atmospheric density, ozone and aerosol.

As shown in Fig. 15, radiation brightness image obtained by MAVI illustrates the radiance stratification phenomenon obviously, which can be used in stratosphere ozone inversion, ozone distribution change monitoring and ozone product accuracy evaluation of similar payloads.

Figure 16 is pseudo color image acquired by FABH. Vertical direction represents different atmosphere from 10 km to 60 km, and horizontal direction represents wavelength (290 nm $\sim$ 1000 nm). As the height increasing, the gradual change and layered phenomenon can be found in Figs. 16 and 17.

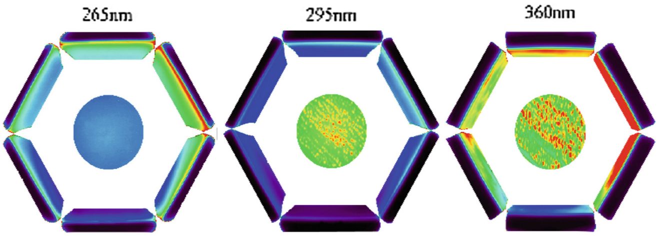

Fig. 15. Radiation brightness image obtained by MAVI on April 11, 2017

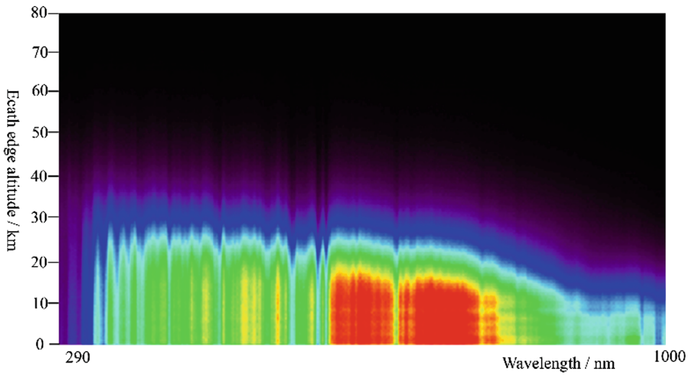

Fig. 16. Atmosphere spectral image obtained by FABH on April 11, 2017

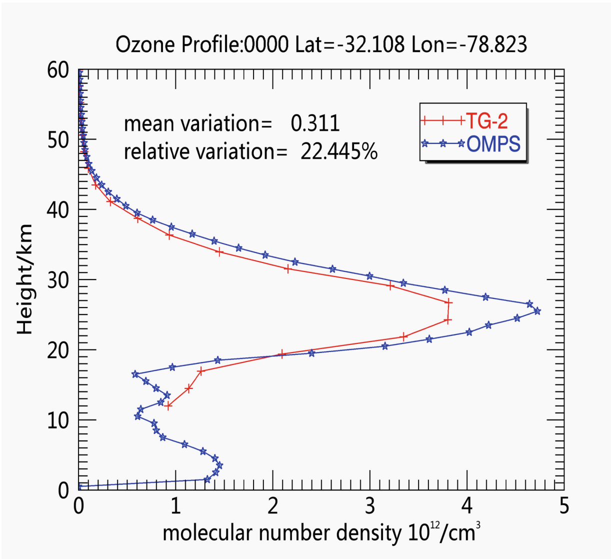

Fig. 17. Comparison between ozone profiles derived from Tiangong-2 and OMPS (2016.12.22)

Based on the algorithm of vertical distribution profile, MUEIS data (vertical spatial resolution: 3 km) has been used to extract the ozone distribution of Pacific Ocean and Beijing. Furthermore, the ozone product of Ozone Mapping Profiler Suite (OMPS) and the data of sounding balloon are used to verify the ozone profile derived from MUEIS data. In the Fig. 18, the mean variation is 0.311, and the relative variation is 22.445%. That is to say, there is a good consistency between MUEIS of Tiangong-2 and OMPS. Further comparison among ozone density (Fig. 18) derived fromTiangong-2, sounding balloon and OMPS was performed. The same result was obtained.

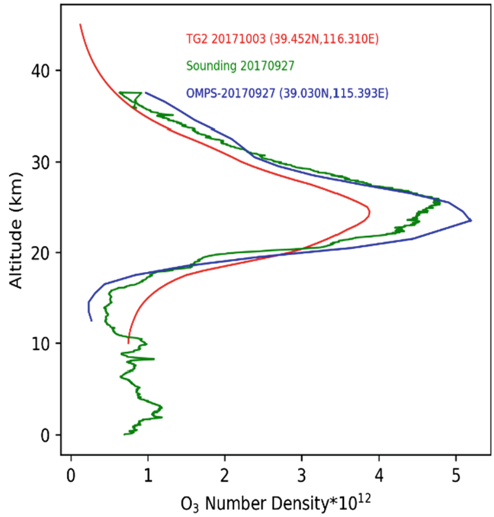

Fig. 18. Comparison of ozone density derived from Tiangong-2, sounding balloon and OMPS (2017.10.03)

5 Conclusion

Tiangong-2 has been in operation for more than two years. Based on advanced earth observation payloads, a large number of high-quality data products have been obtained. Many scientists and application users have utilized these data, which has played an important role in many fields. In the future, the earth observation payloads will continue providing data for research and application. It is expected that more and more valuable results will be achieved.

References

1. Jinghua, W.: China's first space laboratory Tiangong 2 was successfully launched. China Aerospace (10), 9 (2016)
2. Qiong, L.: Black Technology in "Tiangong No. 2". China Economic Report (10), 111–114 (2016)

3. Ji, Y.: The Tiangong 2 is the "most busy" space laboratory. China Aerospace (11), 11–12 (2016)
4. Manned Space Space Application Data Promotion Service Platform. http://www.msadc.cn/rwjstgeh/. Accessed 21 Oct 2018
5. China Manned Space Official Website. http://www.cmse.gov.cn/art/2017/12/11/art_19_32017.html. Accessed 21 Oct 2018
6. Zhiwen, L., Shengyang, L.: Tiangong 2 UV forward spectrometer atmospheric edge height calculation. Optics Precis. Eng. **06**, 1517–1523 (2018)
7. The official website of the Space Application Engineering and Technology Center of the Chinese Academy of Sciences. http://www.csu.cas.cn/gcdt/fzdt/201809/t20180926_5099083.html. Accessed 21 Oct 2018
8. Kang, L.I.U., Bang-yong, Q.I.N., Ling-li, M.U., Sheng-yang, L.I.: Monitoring and analysing of reclamation change based on multi-data remote sensing images: a case study of partial area of Liaoning Province. MARINE Environ. Sci. **36**(06), 911–917 (2017)
9. Jing, X., Dan, M.: Wetland monitoring in Panjin City based on TianGong-2 remote sensing data
10. Kang, L., Bangyong, Q., Shengyang, L.: The application of the Tiangong-2 WIS data in the ecological environment evaluation: a case study of Kunming. In: Proceeding of International Workshop on Environment and Geoscience, June 15–17, Hangzhou, China (2018)
11. Xiaojun, S., Kangyu, F., Jie, W., Wenchao, Q., Xiaolu, L.: Identification of Cotton by Using Random Forest with Tiangong-2 Data
12. Zhuang, Z., Shengyang, L., Yuyang, S., et al.: Early and Late Rice Identification from Tiangong-2 Wide Band Images Based on CNN//Symposium on Electrical, Electronics and Information Engineering, IEEE International (2018)

Design, Performance and In-Orbit Evaluation Results of Tiangong-2 Wide-Band Imaging Spectrometer

Jun Wei[1,4](✉), Lei Ding[1,4], Xianqiang He[2], Yuyu Tang[1,4], Xin Feng[1,4], and Mingsen Lin[3]

[1] Shanghai Institute of Technical Physics, Chinese Academy of Sciences, Shanghai 200083, China
weijun@mail.sitp.ac.cn
[2] State Key Laboratory of Satellite Ocean Environment Dynamics, Second Institute of Oceanography, SOA, Hangzhou 310012, China
[3] National Satellite Ocean Application Service, SOA, Beijing 100081, China
[4] Key Laboratory of Infrared System Detection and Imaging Technology, Chinese Academy of Sciences, Shanghai 200083, China

Abstract. The system design, performance and in-orbit evaluations of a push-broom wide-band imaging spectrometer (WIS) on Tiangong-2 space laboratory is introduced. The WIS has 100 m spatial resolution in ocean color bands (FOV is around 42°), which is the highest compared to other in-orbit ocean color sensors (GOCI, MODIS, VIIRS, and OLCI). Besides, WIS includes visible and near infrared (VNIR), shortwave infrared (SWIR) and thermal infrared (TIR) channels and has excellent performance in ocean color monitoring, and SNR in 0.4–0.8 μm is more than 400 at typical oceanic radiance. Average SNR at SWIR is more than 550 at typical atmosphere radiance. Moreover, the instrument's average NE⊿T at TIR is lower than 20 mK, which is one of the best. The in-orbit tests reveal that the ocean color components retrieved by WIS are highly consistent with the results from the typical ocean color satellite sensors (MODIS, VIIRS and GOCI), but have finer structures due to higher spatial resolution.

Keywords: Tiangong-2 · Wide-band imaging spectrometer
Spectral channel programming · InGaAs detector assembly
HgCdTe detector Dewar assembly

1 Introduction

The WIS is an ocean color remote sensor on Tiangong-2 space laboratory launched on Sep.15, 2016. It has fourteen programmable VNIR channels (V1–V14, 0.40–1.04 μm), two SWIR channels (S1: 1.232–1.252 μm and S2: 1.630–1.654 μm) and two TIR channels (T1: 8.125–8.825 μm and T2: 8.925–9.275 μm), and its spatial resolutions at nadir are 100 m, 200 m and 400 m for the VNIR, SWIR and TIR, respectively. Combining push-broom and multiple module FOV stitch technologies, WIS achieves wide swatch of 300 km.

Y. Gu et al. (Eds.): *Proceedings of the Tiangong-2 Remote Sensing Application Conference*, LNEE 541, pp. 14–27, 2019.
https://doi.org/10.1007/978-981-13-3501-3_2

To meet high performance monitoring over ocean color and temperature of water and sea ice, WIS' radiation has high resolution at each channel, the average signal-to-noise ratio (SNR) in band 0.4–0.8 µm is more than 400 at typical oceanic radiance, average SNR at SWIR is more than 550 at typical atmosphere radiance, and average Noise-equivalent temperature difference (NE⊿T) in TIR is better than 20 mK at 300 K blackbody, which is one of the best among similar ocean sensors in-orbit. Full field of view (FOV) and full aperture on-board calibrator is designed using internal reference radiation source with limited resource. The calibration unit is composed of pointing mirror, surface blackbody and halogen lamp with Pr-Nd glass cover of specific absorption peak. The calibrator rotates the mirror to point to the lamp and blackbody in turn to do the calibration in orbit. In this paper, the details of the design, performance tests and in-orbit evaluations of the WIS are introduced.

2 System

Like MERIS and OLCI of ESA, the WIS is a push-broom remote imaging system. Compared to the optical-mechanical scanning method, the push-broom system has the advantage of improving the system SNR, which is very important for weak ocean color signal detection.

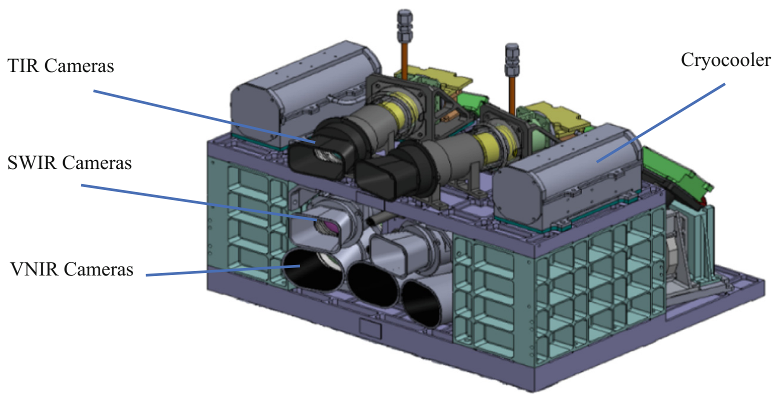

Fig. 1. Layout of the WIS optical head without calibrator

The system consists of an optical head and three control boxes. The optical head, mainly composed of VNIR imaging module, SWIR imaging module, TIR imaging module and calibrator, is the core part of WIS. As shown in the Fig. 1, the three modules are stacked in three layers from bottom to top, and each module is composed of 2 or 3 fan-mounted camera sets with a small FOV overlap.

2.1 VNIR Imaging Module

VNIR imaging module is designed for ocean color and atmospheric correction. Three VNIR cameras are installed fan-shaped to achieve the view of total 42 ° field (about 0.5° field overlap). Each camera is composed of VNIR lens, Spectrograph, CCD array and video electronic unit (Fig. 2). One distinguished characteristic of WIS is the programmability of its VNIR spectral channels in their width and central wavelength. The programming spectral range is 400 ~ 1040 nm with 2.5 nm step. The targets on the earth are first imaged onto the plane of the slit by VNIR lens, and the Spectrograph unit disperses the light through the slit and forms its dispersed image on the CCD array. The 2D array corresponds to the spatial extension of the slit and spectral dispersing dimension.

Seven pieces of lenses construct a transmission optics for VNIR lens. The focal length is 120 mm with F number of 3.2, and optical MTF is 0.85 or higher. The exit pupil of the lens matches the entrance pupil of the spectrograph unit. By integrating reflection and transmission optical design, small spectral bending and spatial distortion are achieved. The linear dispersion rate of the spectrograph is 111 nm/mm, which meets the requirements of system spectral resolution (2.5 nm). The selected CCD (CCD55-30) is a thinned back-illuminated, frame-transfer, non-inverted mode operation CCD from E2 V corp. it's made of 1243 × 576 detector elements, each detector pixel is a 22.5 μm square, corresponding to one pixel in the image. Its dynamic range is better than 96 dB at 1 MHz readout frequency. Mid-band coated is applied to achieve high quantum efficiency in VNIR spectrum [1].

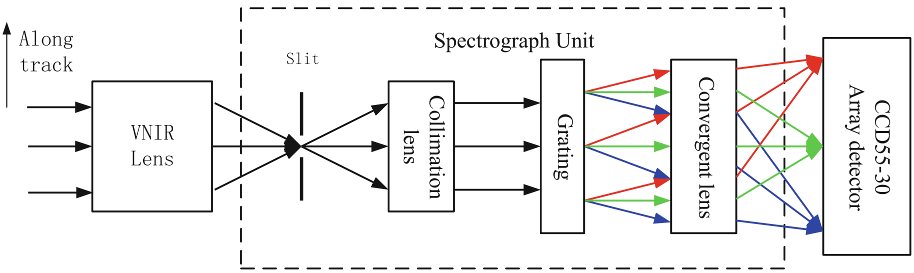

Fig. 2. Diagram of the VNIR camera

2.2 SWIR Imaging Module

SWIR channels aim to monitor cloud-snow and sea-land boundaries as well as to run atmospheric correction of turbid water. To achieve 42° FOV SWIR imaging, two SWIR cameras (FOV 21.5°) are mounted fan-shaped. Each camera is composed of SWIR lens, double band 800 (spatial pixel) *2 (spectral channel) InGaAs detector assembly and signal processing circuit unit. Five pieces of lenses develop the transmission optics of SWIR lens, its focal length is 50 mm with F number of 2.0, and optical MTF is better than 0.85. The SWIR dual-channel InGaAs detector assembly is independently developed by Shanghai Institute of Technical Physics (SITP), Chinese

Academy of Sciences. As shown in Fig. 3. It consists of window, cover plate, filter plate, optical stop, InGaAs focal plane array (FPA), transition electrode plate, thermoelectric cryocooler and metal tube shell. The InGaAs FPA consists of an 800 × 2 responsive elements and readout circuit, which can measure the spectral response of two detection channels by narrow bandpass filter. Responsive element uses a thinned back-illuminated structure, and its size is 25 μm square. Interface of the two channels are mirrored with 1.2 mm distance. Selectable working temperature of 15 °C or 5 °C is guaranteed by way of semiconductor refrigeration. The dark current is less than 5 pA, dynamic range is greater than 80 dB at 1 MHz read frequency, non-uniformity is 3% or less, and there is no blind responsive element.

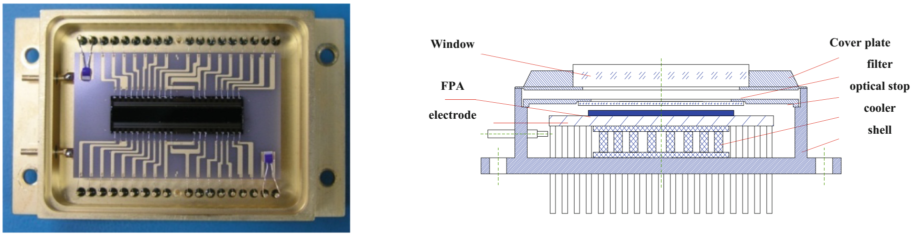

Fig. 3. The photo and schematic of SWIR dual-channel InGaAs detector assembly

2.3 TIR Imaging Module

TIR channels focus on temperature monitoring on sea ice and water. Two TIR cameras with same FOV (21.5°) are combined fan-shaped. Each camera is composed of TIR lens, dual-channel 400 (spatial pixel) × 2 (spectral channel) HgCdTe detector Dewar assembly, Stirling cryocooler and signal processing unit. The Stirling cryocooler can keep 80 K working temperature, and it's independently developed by SITP. Four pieces of lenses form the transmission optics for TIR camera. Its focal length is 28 mm with F number of 1.5, and optical MTF is better than 0.6. The Dewar assembly provides a good low-temperature vacuum environment for the detector, which is

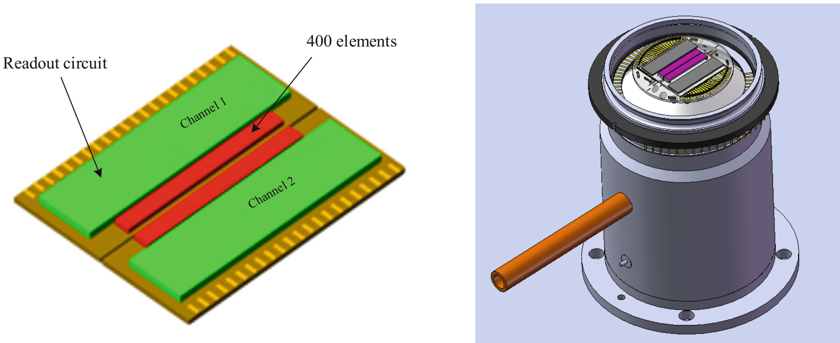

(a) (b)

Fig. 4. (a) Dual-channel TIR FPA (b) Detector Dewar assembly

composed of infrared window, lead ring, shell, core, HgCdTe FPA, infrared filter, cold stop, and degassing agent. The cooling loss is less than 400 mW, and the temperature difference between the cold finger and the FPA is controlled to be under 2 K. As shown in Fig. 4, the FPA detector consists of two monolithically integrated responsive areas (400 elements) and a readout circuit based on capacitive feedback transimpedance amplifier (CTIA). The infrared filter of two spectral channels is installed on two responsive areas by bridge. The responsive element adopts back thinned structure. The size of element is 28 μm square. The D-star(D*) is greater than 8×10^{10} $cmHz^{1/2}W^{-1}$ at 80 K, the non-uniformity is less than 6%, and the responsive area of the detector has no blind element.

Developed by SITP, the TIR camera uses pneumatically driven Stirling cryocooler consisting of compressor and expander unit (Fig. 5). Its cooling capacity is 1.5 W at 80 K FPA temperature, and it takes less than 15 min to drop from room temperature to working temperature inside the Dewar. The lifetime is more than 20,000 h. Each TIR camera is cooled by individual cryocooler. The compressor of each cryocooler is arranged on both sides of the expander unit, and installed with the thermal insulation on the bottom plate. Two heat pipes are installed on the side and the bottom surface of the compressor. The expander uses a single heat pipe to dissipate heat. In order to enhance the overall rigidity of the structure, the location of the compressor is designed to be as low as possible.

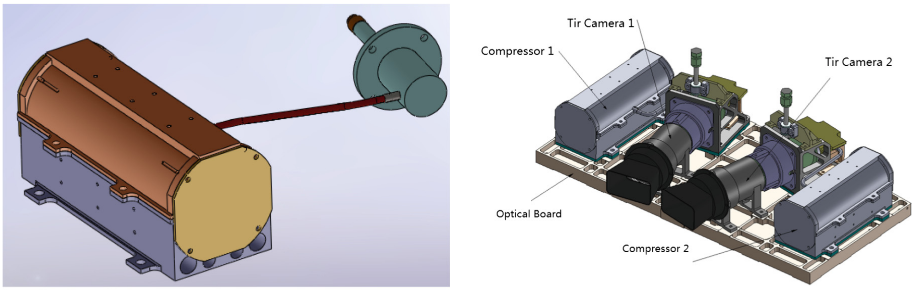

(a) (b)

Fig. 5. (a) Pneumatically driven Stirling cryocooler. (b) Layout of TIR imaging module

2.4 On-Board Calibrator

The On-board calibrator is used to calibrate the system radiation and spectral response during in-orbit operation. The calibrator includes a calibrated mirror mechanism, a halogen lamp box with a Pr-Nd glass cover plate, a temperature control surface blackbody and a VNIR/SWIR calibration detectors unit.

As shown in Fig. 6, the in-orbit calibration was fulfilled by moving the calibration pointing mirror to point to different positions. At position 1, it targets at the surface blackbody, starting temperate control process and during cooling down, select two to three control points with relatively steady temperature for TIR calibration. At position 2, the halogen lamp box with Pr-Nd glass cover plate is targeted. By opening and closing the six halogen lamp sources with various combinations, we can get three radiation levels for VNIR and SWIR calibration. At the same time, the spectral absorption peak generated from the same lamp sources passing through the Pr-Nd glass is utilized for spectrum calibration using envelop detection algorithm. During normal ground observation, the pointing mirror is at position 3, ensuring that the imaging field is not obstructed. The VNIR and SWIR bands are each equipped with a set of full-spectrum calibration detectors for monitoring the long-term stability of the lamp source.

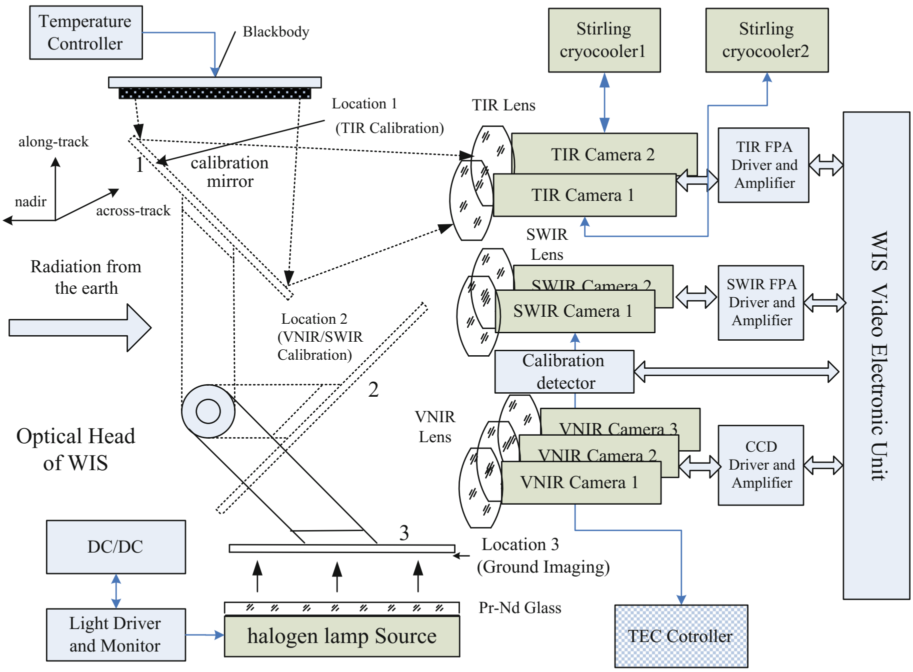

Fig. 6. Diagram of Optical head of the WIS

2.5 VNIR in-Orbit Spectral Channel Programming

The 14 VNIR spectrum channels of WIS support in-orbit programming of spectral center wavelength and bandwidth, which has significant advantages including improving the efficiency of the instrument when the data transmission rate is limited, carrying out in-orbit spectrum research for specific target; correcting the spectral properties of channels when they alter in orbit [2].

(1) Implementation

The target is imaged on the slit of the spectrograph unit through the lens (Fig. 2). The light passing through the slit is dispersed into 2D spectral and spatial images by the spectrograph and cast to the area-array CCD.